ELSEVIER

Thermochimica Acta 372 (2001) 129–136

thermochimica acta

www.elsevier.com/locate/tca

Thermodynamic and conformational properties of DNA triplexes containing 3′,3′-phosphodiester bond

Concetta Giancola[a,*], Maria Pieri[a], Luigi Petraccone[a], Daniela Montesarchio[b], Guido Barone[a]

[a]*Department of Chemistry, University "Federico II" of Naples, Complesso Universitario di Monte Sant'Angelo, Via Cintia, 80126 Naples, Italy*

[b]*Department of Organic and Biological Chemistry, University "Federico II" of Naples, Complesso Universitario di Monte Sant'Angelo, Via Cintia, 80126 Naples, Italy*

Received 18 October 2000; accepted 11 January 2001

Abstract

The thermodynamic characterization of the stability of two DNA triple helices of alternate sequence was obtained by differential scanning calorimetry (DSC). The conformational properties of these triple helices were investigated by circular dichroism (CD) and molecular mechanics. The triplexes under investigation form by way of major groove Hoogsteen association of a Watson–Crick 16-mer duplex with an all pyrimidine 16-mer or 15-mer third strand. The target duplex is composed of two adjacent oligopurine–oligopyrimidine domains where oligopurine sequences alternate on the two duplex strands. Both the third strands contain a 3′,3′-phosphodiester junction, which introduces the appropriate inversion of polarity and let the switch from one oligopurine strand of the duplex to the other. The two-third strands differ for the lack of a cytidine monophosphate in the junction region. Thermal denaturation profiles indicate the initial loss of the third strand followed by the dissociation of the target duplex with increasing temperature. Transition enthalpies, entropies and free energies were derived from DSC measurements. The comparison of Gibbs energies reveals that a more stable triplex is obtained when in the third strand there is the lack of one nucleotide in the junction region. The thermodynamic data were discussed in relation to structural models.

Keywords: Thermodynamic stability; DNA triple helices; Differential scanning calorimetry; Circular dichroism; Molecular modeling

1. Introduction

The interest in triple helices has been rapidly growing, especially during the past decade, essentially for two reasons. Firstly, the discovery of H-form DNA, a triplex-containing structure, observed in vivo under torsional stress within DNA sequences with mirror symmetry [1]. Secondly, oligonucleotide-directed triple helix formation is a unique way to design specific ligands that recognize and selectively target regions in double-stranded DNA [2], thus opening up a wide field of applications in medicine and biotechnology. Numerous attempts have been made to use oligonucleotides, particularly triple-helix-forming oligonucleotides (TFO) as tools for exploring DNA structure and for creating methods for regulation of gene expression and genome analysis.

* Corresponding author. Tel.: +39-81-674266.
E-mail address: giancola@chemistry.unina.it (C. Giancola).

0040-6031/01/$ – see front matter
PII: S0040-6031(01)00448-8

Oligonucleotides of defined sequence can bind to the major groove of double-helical DNA to form triple helices by recognition of the oligopurine-rich strand [3,4]. This recognition process is extremely simple, efficient and specific, being based on sequence-specific hydrogen bonding: pyrimidine-rich triplex forming oligonucleotides target in a parallel orientation homopurine fragments in double-stranded DNA by Hoogsteen T-A•T and C-G•C^+ triplets formation [5,6], while homopurine can recognize in an antiparallel orientation the purine strand of the Watson–Crick duplex upon generation of T-A•A and C-G•G triads [7] (here '-' and '•' indicate the Watson–Crick and Hoogsteen hydrogen bonds, respectively). The formation of the triad C-G•C^+ requires the protonation of the N_3 of cytosine in the third strand. The stability of the triplexes and the efficiency of their formation are significantly affected by the nature and the concentration of mono and divalent cations, pH, temperature, the triplex structure and base composition, the length of the ligands [1,8–12]. In order to be selective for a unique recognition and to form stable triplexes, the DNA target sequences were originally limited to relative long oligopurine–oligopyrimidine tracts, at least 16–17 consecutive bases, for the human genome. In an effort of extending the range of triplex forming DNA tracts, Singleton and Dervan [13] and Ono et al. [14] investigated the ''alternate strand approach'' to recognize alternating and adjacent oligopurine–oligopyrimidine tracts, the designed TFO crosses the double helix major groove, switching from one purine strand to the other. The third strand switch can occur preserving or inverting its chain polarity. For a correct Hoogsteen triplets formation, the TFO must have an appropriate inversion of polarity in correspondence of the junction between the homopurine and the homopyrimidine sequences of the duplex; in this way the third homopyrimidine strand remains parallel to each homopurine domain [15]. In this case a convenient linker must be introduced for the appropriate inversion of polarity, i.e. a 3′,3′- or a 5′,5′-internucleoside junction, which assures for both 5′- and 3′-ends the required orientation [13–17].

Previous studies have suggested that blocks of CGC^+ triplets are unstable because of repulsion between the adjacent positive charges [18] and the stacking energies decrease in the order TAT/CGC^+, TAT/TAT and CGC^+/CGC^+ [19]. So the alternate sequences are the most stable. Moreover, alternate third strands involving only a bridging phosphate between the two 3′-ends of oligopyrimidine domains [20], as well as 3′,3′- or 5′,5′-linkages [17,21], bind to their double-stranded target with variable stabilities. Pronounced stability increases have been reported only with 3′,3′-junctions [17,20–22]. Consequently, we focused our attention on triple helices of alternate sequence, in which the third strand contains a 3′,3′-phosphodiester junction.

The present work is devoted to the comparison of thermodynamic stability of two triple helices containing a 16-mer double helix and a 16-mer or 15-mer third strand, named 16-mer and 15-mer triplexes, respectively. In the 15-mer structure the target double helix contains one base pair (C-G) that does not participate in Hoogsteen base pair interactions and it is spanned by the linker. In the 16-mer structure all the duplex base pairs potentially form Hoogsteen base pair interactions (Fig. 1).

We have used differential scanning calorimetry, circular dichroism and molecular mechanics to characterize the triple helix formation. The thermodynamic data are discussed in relation to structural models. Compiling the requisite body of thermodynamic data is a minimum first step toward making the development and expanded use of oligonucleotides for

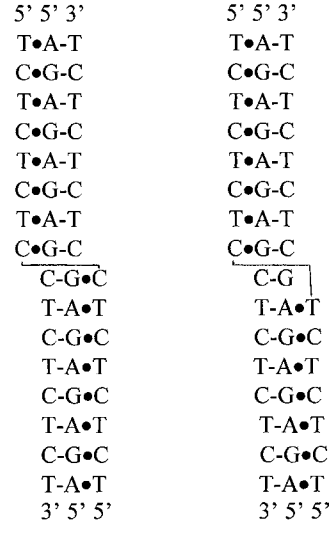

Fig. 1. Schematic representation of the 16-mer triplex (on the left) and the 15-mer triplex. The symbols '-' and '•' indicate the Watson–Crick and the Hoogsteen hydrogen bonds, respectively.

modulating biochemical activities through site-specific triplex formation.

2. Materials and methods

2.1. Triple helices preparation

The 3′,5′-oligodeoxyribonucleotide was synthesized using standard solid-phase phosphoramidite methods [23]. The third strands containing a 3′,3′-phosphodiester junction have been conveniently synthesized trough a solid phase procedure involving only 3′-phosphoramidite nucleosides, and starting from a modified support that links the first nucleotide through the base [24].

The triplexes were formed by mixing stoichiometric amounts of oligonucleotides in the appropriate buffer and heating the solution at 90°C for 5 min. The solution was slowly cooled to room temperature, then equilibrated for 1 day at 4°C before performing DSC experiments.

The buffer used was 140 mM KCl, 5 mM NaH_2PO_4 and 5 mM $MgCl_2$. Potassium chloride (Sigma), monosodium phosphate (Sigma) and magnesium chloride (Carlo Erba) were used as obtained from commercial suppliers. The concentration of oligonucleotide solutions was determined spectrophotometrically, using the extinction coefficients at 260 nm calculated by a nearest neighbor model [25]. The pH of solutions was measured using a Radiometer pH meter model PHM 93 at 25°C.

2.2. Differential scanning calorimetry

Differential scanning measurements were performed with a Setaram Micro-DSC. Scannings from 0 to 95°C and vice versa at the rate of 0.5°C min^{-1} were done. The calorimeter was interfaced to an IBM PC computer for automatic data collection and analysis using a software previously described [26]. The triplex concentration employed was 7.2×10^{-5} M. The excess heat capacity function $\langle \Delta C_p \rangle$ was obtained after baseline subtraction, assuming that the baseline is given by the linear temperature dependence of the native state heat capacity [27].

The transition enthalpies, $\Delta H^0(T_m)$, were obtained by integrating the area under the heat capacity versus temperature curves. T_m is the temperature corresponding to the maximum of each DSC peak. The transition entropies, $\Delta S^0(T_m)$, were determined by integrating the curve obtained by dividing the heat capacity curve by the absolute temperature.

2.3. CD measurements

Circular dichroism spectra were obtained with a JASCO 715 circular dichroism spectrophotometer equipped with thermostatically cuvette holder (JASCO PTC-348), which allows measurements at controlled temperature. Quartz cuvettes with 1 mm optical path length were used. The CD spectra were recorded from 340 to 200 nm at 5°C and normalized by subtraction of the background scan with buffer. The molar ellipticity was calculated from the equation $[\vartheta] = \vartheta/cl$, where ϑ is the relative intensity, c the concentration of oligonucleotides and l is the path length of the cell (cm). The instrument was calibrated with an aqueous solution of D-10-(+)-camphorsulfonic acid at 290 nm [28]. CD spectra were recorded with a response of 16 s, a 2.0 nm band width and a scan rate of 5 nm min^{-1} and were averaged over at least five scans.

2.4. Molecular modeling

The initial structures of the two triplexes were generated from the helical co-ordinates given by Liu [29], who reported a B-like conformation for the duplex portion in a triplex. The two oxygen atoms in the 3′-position at the junction site of the third strand were linked by a phosphate residue. The charges on the atoms of protonated cytosines were reassessed in order to take into account the protonation. The two triplexes were made electrically neutral by addition of sodium counterions and then, any triplex individually was placed in a box 30.1 Å × 30.1 Å × 56.1 Å of Monte Carlo TIP3P [30] water, with periodic boundary conditions. The water molecules that were nearest of 2.3 Å from any solute atoms were removed. For both the triple helices the same minimization procedure was used. The Amber force field [31] was utilized and a cut-off of 12 Å was applied to the non-bonded potential. Energy minimization was performed using 1500 steps of the steepest descent method followed by the conjugate gradient method until convergence to a RMS gradient of 0.1 kcal mol^{-1} $Å^{-1}$.

Table 1
Thermodynamic parameters of the two triple helices and of the double helix at pH 6.6

	Transition[a]	T_m[b] (°C)	$\Delta H^0(T_m)$ (kJ mol^{-1})	$\Delta S^0(T_m)$ (kJ mol^{-1} K^{-1})
15-mer triplex	I	26.0	156 ± 9	0.437 ± 0.02
	II	69.0	440 ± 14	1.200 ± 0.07
16-mer triplex	I	23.0	115 ± 12	0.303 ± 0.03
	II	68.8	436 ± 8	1.190 ± 0.04
16-mer duplex		69.0	437 ± 15	1.190 ± 0.05

[a] Transition I: $A_2B \Leftrightarrow A_2 + B^*$; transition II: $A_2 \Leftrightarrow 2A^*$.
[b] The error in T_m does not exceed 0.2°C.

3. Results and discussion

3.1. Thermodynamics of triple helix formation

The thermal stability of the two triple helices was studied at pH 6.6, keeping the concentration constant at 7.2×10^{-5} M. The thermodynamic data are collected in Table 1 and the calorimetric profiles are shown in Fig. 2. The triplexes melt in two sequential well resolved steps. The thermal denaturation is a reversible, not kinetically limited process. In fact, scansions at different rate were performed as follows: increasing or decreasing the scanning rate to 1 or to 0.3 K min^{-1}, respectively, any variation in the thermodynamic parameters was obtained. The low temperature transition is attributable to the release of the third strand from the target double helix. The high temperature transition is relative to the dissociation of the double helix, in fact under comparable conditions this transition coincides exactly with the melting transition of the free double helix. Hence, the overall process can be represented according to the following scheme:

$$A_2B \Leftrightarrow A_2 + B^*$$

$$A_2 \Leftrightarrow 2A^*$$

where A_2B indicates the triplex, A_2 the target duplex, A^* indicates both the complementary denatured single strands, B the third strand and B^* represents the denatured state.

Inspection of enthalpy data reported in Table 1 reveals that the enthalpy changes associated with

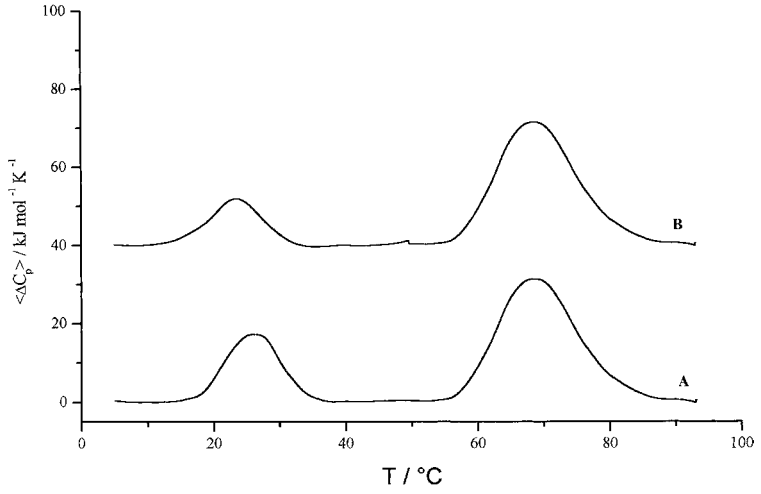

Fig. 2. DSC profiles of the 15-mer triplex (A) and 16-mer triplex (B) at pH 6.6. The sample concentrations were 7.2×10^{-5} M. Excess capacity values have been shifted along the *y*-axis for ease presentation.

the second transition of the 15-mer and 16-mer triplexes, 440 and 436 kJ mol^{-1}, respectively, are in good agreement with the enthalpy change of the free double helix, 435 kJ mol^{-1}. These values are in satisfactorily agreement with the predicted enthalpy change of 444 kJ mol^{-1} calculated from a nearest neighbor analysis, according to the method of Santalucia et al. [32]. The van't Hoff enthalpies have been obtained by DSC profiles utilizing the following equation:

$$\Delta H_{\mathrm{vH}} = 6RT_{\mathrm{m}}^2 \frac{\langle \Delta C_p(T_{\mathrm{m}}) \rangle}{\Delta H^0(T_{\mathrm{m}})}$$

where T_{m} is the maximum of DSC peak and corresponds to a dissociation degree of 0.5, $\langle \Delta C_p(T_{\mathrm{m}}) \rangle$ is the value of the excess heat capacity function at T_{m} and $\Delta H^0(T_{\mathrm{m}})$ is the calorimetric enthalpy directly obtained by the area under DSC peak. The coefficient 6 originates by the stoichiometry of dissociation [33]. The close correspondence between the calorimetric and van't Hoff enthalpies of the second process supports the assumption that the reaction follows a two-state process in which intermediate states are not significantly populated.

For the lower temperature transition the van't Hoff enthalpy is larger than the calorimetric enthalpy, as already found for melting experiments involving DNA triple helices [34–38]. Really, the aggregation phenomenon or the kinetic effects cannot satisfactorily account for the apparent inconsistency in the enthalpy data from calorimetric and van't Hoff analyses, as also reported by Plum et al. [39].

The calorimetric data reveal that the 15-mer triplex is thermally more stable than the 16-mer triplex, the transition maximum temperature being 26 and 23°C, respectively. The transition enthalpy and entropy of 15-mer triplex are also greater then 16-mer triplex ones, $\Delta\Delta H^0$ is 41 kJ mol^{-1} and $\Delta\Delta S^0$ is 123 J mol^{-1} K^{-1}. In order to obtain the relative stability of the triple helices, ΔG^0 values were calculated at 298 K assuming a negligible difference in transition heat capacity. The calorimetric profiles, in fact, do not show significant ΔC_p for both the triple helices, as already found for triplex transitions by different authors [37,38,40,41]. The calculation gives a $\Delta\Delta G^0$ value of 4.3 kJ mol^{-1}, i.e. the 15-mer triplex is thermodynamically more stable than the 16-mer triplex, with a difference in the stability of 17%.

3.2. CD spectra of the triplexes

Circular dichroism spectra of the triplexes, double helix and of the 15-mer single strand are displayed in Fig. 3. The 16-mer single strand spectrum is super-

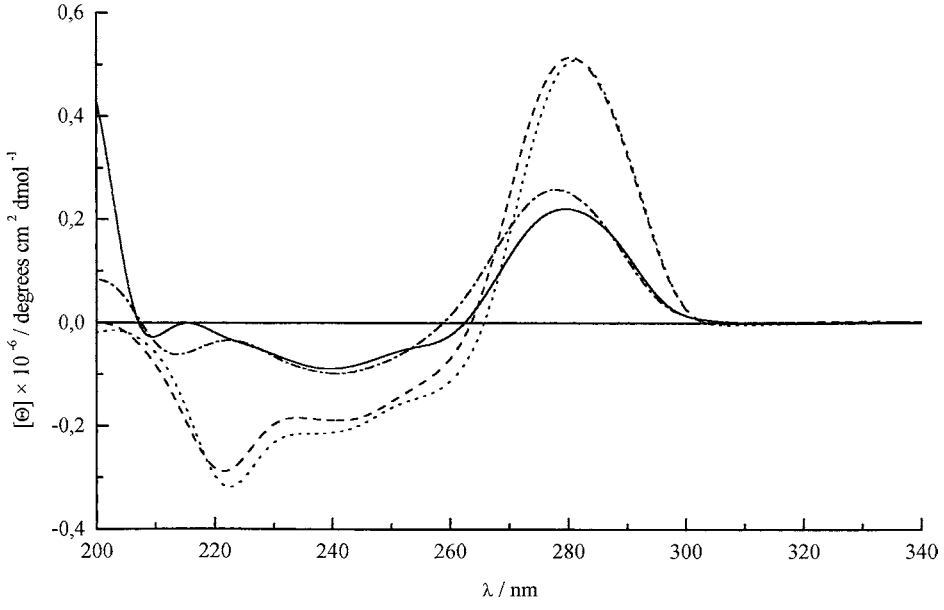

Fig. 3. CD spectra of the 16-mer duplex (solid line), of the 15-mer third strand (dash dotted line), of the 15-mer triplex (dashed line) and of the 16-mer triplex (dotted line) at pH 6.6. All the spectra were recorded at 5°C.

imposable to that of the 15-mer single strand (spectrum not shown) and both of them have the typical shape of single-stranded DNA [42].

The CD spectrum of the double helix is consistent with the B-form duplex DNA [43,44]. The two spectra of the triplexes are close to the spectrum of poly[d(C^+-T)•d(A-G)•d(C-T)] triplex reported by Antao et al. [45]. These spectra show slight differences attributable to non equivalent conformations in solution.

3.3. Molecular modeling studies

In order to gain information on the molecular geometry of the two triple helices, especially of the junction region, molecular mechanics calculations were performed. The molecular models of the two triplexes are shown in Fig. 4. Initially, two different calculations were performed, one with full inclusion of water, counterions and using a unitary dielectric constant, the other with a simpler representation without explicit water accounted. The results obtained depend on how electrostatic and solvent-associated effects are taken into account. In the representation without water there were ends fraying effects; moreover, the presence of the water molecules, particularly in the junctions region, is essential to determine the geometry of the system. Indeed, some water molecules are enclosed in the cavity of the junction site in the 15-mer triplex, establishing hydrogen bonds with the base pairs of the duplex region. The calculation was then performed with explicit water.

The most streaking results are (i) in the 15-mer triplex structure all the bases of the single strand form the Hoogsteen base pair interactions, even if one base

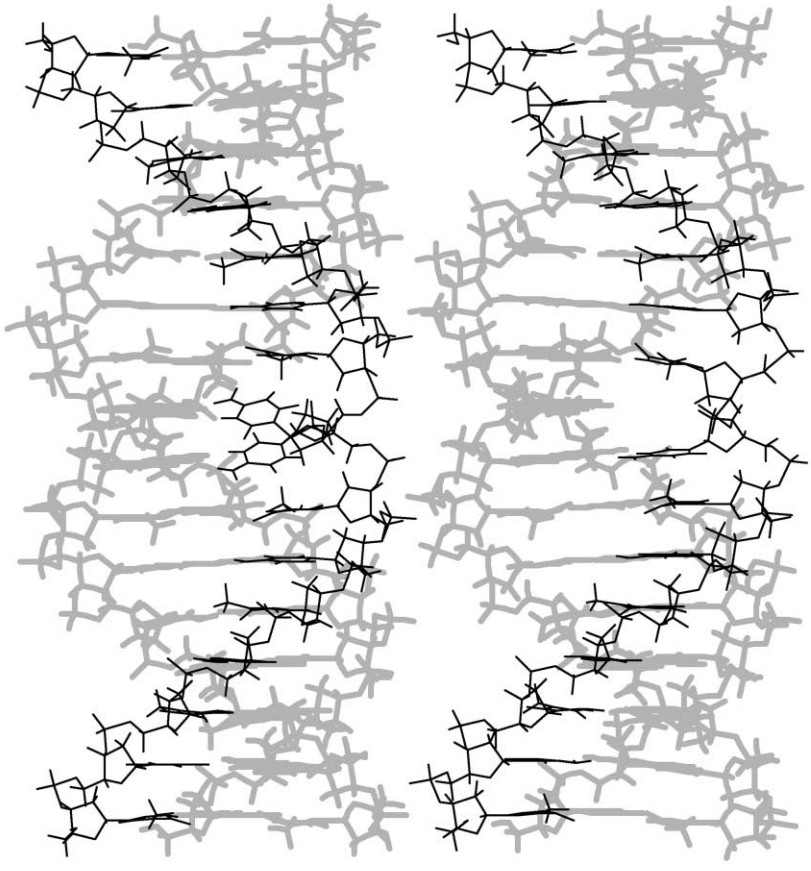

Fig. 4. Triple helical structure of the 16-mer triplex (on the left) and the 15-mer triplex obtained by molecular mechanics. The Watson–Crick strands are grey, and the third strands are black.

pair (C-G) of the target double helix does not participate in Hoogsteen hydrogen bonds and (ii) in the 16-mer triplex structure the two bases of the third strand directly bonded to the linker do not form the Hoogsteen base pair interactions. Hence, in the 15-mer triplex the lack of one nucleotide in the junction point reduces the internal tensions and the third strand is able to adapt its geometry to the double helix one without causing any distortion.

4. Conclusions

The two triple helices under investigation differ between each other for the absence of a cytidine monophosphate in the third strand of the 15-mer triplex and show different physico-chemical properties at pH 6.6. The calorimetric data reveal that the 15-mer triplex exhibits a T_m 3°C higher than the 16-mer triplex. The ΔG^0 calculations show that the 15-mer triplex is thermodynamically more stable. Molecular modeling of the two macromolecules, obtained by molecular mechanics, suggests an interpretation of the thermodynamic data. As already illustrated, in the junction region of the 16-mer triplex structure a strongest distortion is present. Specifically, the two bases bonded to the linker lose the correct orientation to form the Hoogsteen hydrogen bonds. On the contrary, in the 15-mer triplex all the bases of the third strand form the triads. In conclusion, the molecular modeling studies indicate that in the 15-mer triplex a greater number of hydrogen bonds and stacking interactions are retained. This could justify the differences in ΔH^0. Furthermore, the major gain in the transition entropy of the 15-mer triplex is consistent with the molecular geometry, which reveals that this triple helix assumes a more compact structure if compared with that of 16-mer triplex. Hence, it can be concluded that with a 3′,3′-phosphodiester junction more stable triplexes can be obtained when in the third strand there is the lack of one nucleotide in the junction region.

Acknowledgements

This work was supported by a PRIN-MURST grant from the Italian Ministry of University and Scientific and Technological Research (Rome).

References

[1] S.M. Mirkin, V.I. Lyamichev, K.N. Drushlyak, V.N. Dobrynin, S.A. Filippov, M.D. Frank-Kamenetskii, Nature 330 (1987) 495.
[2] C. Giovannangeli, C. Hélène, Antisense Nucl. Acid Drug Develop. 7 (1997) 413.
[3] H.E. Moser, P.B. Dervan, Science 238 (1987) 645.
[4] T. Le Doan, L. Perroult, D. Praseuth, N. Habhounb, J.-L. Decout, N.T. Thoung, J. Lhomme, C. Hélène, Nucl. Acids Res. 15 (1987) 7749.
[5] G. Felsenfeld, D.R. Davies, A. Rich, J. Am. Chem. Soc. 79 (1957) 2023.
[6] K. Hoogsteen, Acta Crystallogr. 12 (1959) 822.
[7] P.A. Beal, P.B. Dervan, Science 251 (1991) 1360.
[8] B.H. Johnston, Science 248 (1988) 1800.
[9] S.F. Singleton, P.B. Dervan, Biochemistry 31 (1992) 10995.
[10] S.F. Singleton, P.B. Dervan, Biochemistry 32 (1993) 13171.
[11] V. Malkov, O. Voloshin, V.N. Soyfer, M.D. Frank-Kamenetskii, Nucl. Acids Res. 21 (1993) 585.
[12] D.A. Horne, P.B.J. Dervan, J. Am. Chem. Soc. 112 (1990) 2435.
[13] S.F. Singleton, P.B.J. Dervan, J. Am. Chem. Soc. 116 (1994) 10376.
[14] A. Ono, C.N. Chen, L. Kan, Biochemistry 30 (1991) 9914.
[15] D.M.G. Gowers, K.R. Fox, Nucl. Acids Res. 27 (1999) 1569.
[16] B.C. Froehler, T. Terhorst, J.P. Shaw, S.N. McCurdy, Biochemistry 31 (1992) 1603.
[17] B.W. Zhou, C. Marchand, U. Asseline, N.T. Thuong, J.S. Sun, T. Garestier, C. Hélène, Bioconjugate Chem. 6 (1995) 516.
[18] L.L. Kiessling, L.C. Griffin, P.B. Dervan, Biochemistry 31 (1992) 2829.
[19] J. Chomilier, J.-S. Sun, D.A. Collier, T. Garestier, C. Hélène, R. Lavery, Biophys. Chem. 45 (1992) 143.
[20] L. De Napoli, A. Messere, D. Montesarchio, A. Pepe, G. Piccialli, M. Varra, J. Org. Chem. 62 (1997) 9024.
[21] U. Asseline, N.T. Thuong, Tetrahedron Lett. 35 (1994) 5221.
[22] B.C. Froehler, T. Terhorst, J.-P. Shaw, S.N. McCurdy, Biochemistry 31 (1992) 1603.
[23] M. Gait, Oligonucleotide Synthesis: A Practical Approach, IRL Press, Oxford, UK, 1984.
[24] L. De Napoli, G. Di Fabio, A. Messere, D. Montesarchio, D. Musumeci, G. Piccialli, Tetrahedron 55 (1999) 9899.
[25] C.R. Cantor, M.M. Warshaw, H. Shapiro, Biopolymers 9 (1970) 1059.
[26] G. Barone, P. Del Vecchio, D. Fessas, C. Giancola, G. Graziano, J. Thermal Anal. 39 (1993) 2779.
[27] E. Freire, R.L. Biltonen, Biopolymers 17 (1978) 1257.
[28] J.T. Yang, C.S.C. Wu, H.N. Martinez, Methods Enzymol. 130 (1986) 208.
[29] K. Liu, V. Sasisekharan, H.T. Miles, G. Raghunathan, Biopolymers 31 (1996) 10671.
[30] W.L. Jorgensen, J. Chandrasekhar, J.D. Madura, R.W. Impey, M.L. Klein, J. Chem. Phys. 79 (1983) 926.
[31] W.D. Cornell, P. Cieplak, C.I. Bayly, I.R. Gould, K.M. Merz, D.M. Ferguson, D.C. Spellmeyer, T. Fox, J.W. Caldewell, P.A. Kollman, J. Am. Chem. Soc. 117 (1995) 5179.

[32] J. Santalucia, H.T. Allawi, P.A. Seneviratne, Biochemistry 35 (1996) 3555.
[33] K.J. Breslauer, in: H.J. Hinz (Ed.), Thermodynamic Data for Biochemistry and Biotechnology, Springer, Berlin, 1986, Chapter 15, p. 402.
[34] E.G. Plum, Y.-W. Park, S.F. Singleton, P.B. Dervan, K.J. Breslauer, Proc. Natl. Acad. Sci. U.S.A. 87 (1990) 9436.
[35] G. Manzini, L.E. Xodo, D. Gasparotto, F. Quadrifoglio, G.A. van der Marel, J.H. van Boom, J. Mol. Biol. 213 (1990) 833.
[36] J. Völker, D.P. Botes, G.G. Lindsey, H.H. Klump, J. Mol. Biol. 230 (1993) 1278.
[37] H.P. Hopkins, D.D. Hamilton, W.D. Wilson, G.J. Zon, Phys. Chem. 97 (1993) 6555.
[38] G.E. Plum, K.J. Breslauer, J. Mol. Biol. 248 (1995) 679.
[39] E.G. Plum, D.S. Pilch, S.F. Singleton, K.J. Breslauer, Annu. Rev. Biophys. Biomol. Struct. 24 (1995) 319.
[40] P.V. Scaria, R.H. Shafer, Biochemistry 35 (1996) 10985.
[41] C. Giancola, A. Buono, G. Barone, L. De Napoli, D. Montesarchio, D. Palomba, G. Piccialli, J. Thermal Anal. Cal. 56 (1999) 1177.
[42] D.M. Gray, R.L. Ratliff, M.R. Vaughan, Methods Enzymol. 211 (1992) 389.
[43] K.I. Ivanov, L.E. Minchenkova, E.E. Minyat, M.D. Frank-Kamenetsckii, A.K. Schyolkina, 87 (1974) 817.
[44] C.A. Bush, Basic Principles Nucl. Acid Chem. 2 (1974) 91.
[45] V.P. Antao, A.N. Lane, J. Dhesi, S. Bergqvist, T.J. Brown, J. Mol. Biol. 275 (1998) 811.